AMERICAN ACADEMY OF OPHTHALMOLOGY®

In partnership with the AMERICAN GLAUCOMA SOCIETY

Predicting Glaucoma before Onset Using Deep Learning

Anshul Thakur, PhD,[1,2] *Michael Goldbaum, MD, MSc,*[3] *Siamak Yousefi, PhD*[2,4]

Purpose: To assess the accuracy of deep learning models to predict glaucoma development from fundus photographs several years before disease onset.

Design: Algorithm development for predicting glaucoma using data from a prospective longitudinal study.

Participants: A total of 66 721 fundus photographs from 3272 eyes of 1636 subjects who participated in the Ocular Hypertension Treatment Study (OHTS) were included.

Main Outcome Measures: Accuracy and area under the curve (AUC).

Methods: Fundus photographs and visual fields were carefully examined by 2 independent readers from the optic disc and visual field reading centers of the OHTS. When an abnormality was detected by the readers, the subject was recalled for retesting to confirm the abnormality and for further confirmation by an end point committee. By using 66 721 fundus photographs, deep learning models were trained and validated using 85% of the fundus photographs and further retested (validated) on the remaining (held-out) 15% of the fundus photographs.

Results: The AUC of the deep learning model in predicting glaucoma development 4 to 7 years before disease onset was 0.77 (95% confidence interval [CI], 0.75−0.79). The accuracy of the model in predicting glaucoma development approximately 1 to 3 years before disease onset was 0.88 (95% CI, 0.86−0.91). The accuracy of the model in detecting glaucoma after onset was 0.95 (95% CI, 0.94−0.96).

Conclusions: Deep learning models can predict glaucoma development before disease onset with reasonable accuracy. Eyes with visual field abnormality but not glaucomatous optic neuropathy had a higher tendency to be missed by deep learning algorithms. *Ophthalmology Glaucoma 2020;■:1−7 © 2020 by the American Academy of Ophthalmology. This is an open access article under the CC BY-NC-ND license (http://creativecommons.org/licenses/by-nc-nd/4.0/).*

Although most of the application of deep learning models has been centered around glaucoma diagnosis for the screening purposes, the aim of our study is to evaluate the utility of deep learning models for prediction of glaucoma from color fundus photographs well before the manifestation of the clinical signs. We hypothesize that deep learning models, such as models that we propose, can uncover clinical and subclinical glaucoma-induced signs that may lead to improving our understanding of mechanisms underlying glaucoma.

Glaucoma is a heterogeneous group of disorders that represents the second leading cause of blindness overall, affecting up to 91 million individuals worldwide.[1,2] Glaucoma has multiple known risk factors, including older age, African-American ethnicity, elevated intraocular pressure (IOP), and thinner central corneal thickness.[3,4] However, subjects with 1 or more of these risk factors may or may not develop glaucoma, making an accurate prediction challenging.[5] Because glaucoma can be asymptomatic, its detection before significant vision loss is critical.[6] Thus, methods for predicting glaucoma could have a significant impact on public health.

Dilated fundus photography provides a convenient and inexpensive means for recording optic nerve head structure, and glaucomatous optic neuropathy (GON) assessment remains a gold standard for indicating the presence of glaucoma.[7,8] However, manual assessment of the optic disc through fundus photographs for glaucoma screening requires significant clinical training, is highly subjective with currently limited agreement regarding results even among glaucoma specialists, and is labor intensive for application to the general population.[9,10] Recent advances in artificial intelligence and deep learning models along with significant growth in available methods to record fundus photographs have shown promise and allowed the development of objective systems to assess the optic nerve head through fundus photographs, thus leading to enhanced glaucoma diagnosis (Norouzifard M, Nemati A, GholamHosseini H, et al. Automated glaucoma diagnosis using deep and transfer learning: proposal of a system for clinical testing. Paper presented at: 2018 International Conference on Image and Vision Computing New Zealand (IVCNZ). November 19-21, 2018, Auckland, New Zealand).[11-14]

Deep learning models require large clinically annotated training datasets to learn promising features from the images. Learning from data has advantages over predefined assumptions and rules to build the knowledge in machine learning classifiers. Several studies have shown that deep learning models can identify disease-induced signs to

https://doi.org/10.1016/j.ogla.2020.04.012
ISSN 2589-4196/20

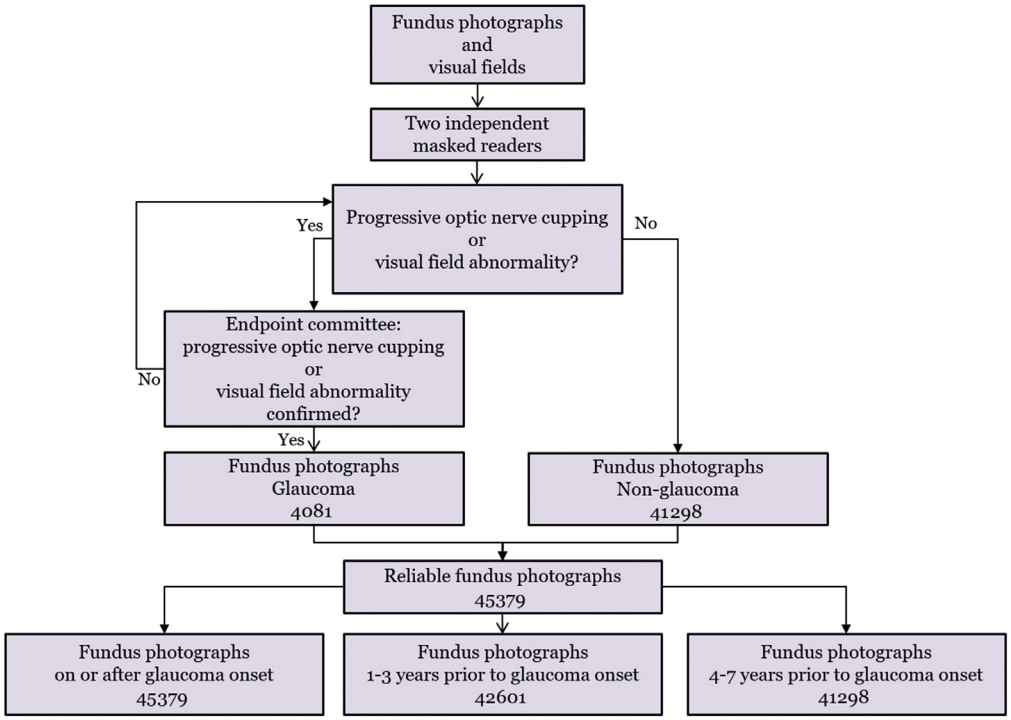

Figure 1. Flowchart of glaucoma identification and labeling. The eye is labeled as glaucoma based on glaucomatous optic neuropathy (GON) or visual field abnormality. Reading center assignment should be further confirmed by an end point committee. Three datasets were selected from fundus photographs based on glaucoma onset date of each eye: 1 dataset for glaucoma diagnosis and 2 datasets for glaucoma prediction.

diagnose disease or identify the severity of disease from ophthalmic images with high accuracy in ocular conditions such as diabetic retinopathy, age-related macular degeneration, and glaucoma.[13,15-19] Integrating deep learning models into portable fundus photography cameras or general practice may provide automated assessment of ocular conditions such as glaucoma and has a significant potential for providing affordable screening of at-risk populations and improving access to care.

Methods

Participants and Data

The fundus photographs of this study were obtained from the Ocular Hypertension Treatment Study (OHTS) after signing the data use agreement and receiving Institutional Review Board approval. The study was conducted according to the tenets of Helsinki. All participants provided informed consent. The OHTS was a prospective, multicenter investigation (22 centers across the United States) that sought to prevent or delay the onset of visual field loss in patients with elevated IOP (at moderate risk of developing glaucoma). All risk factors were measured at the baseline before disease onset and were collected for approximately 16 years (phases 1 and 2). Thus, the longitudinal basis of the OHTS dataset allows development of models for predicting glaucoma before disease onset.

A total of 66 721 fundus photographs from 3272 eyes of 1636 subjects with normal-appearing optic disc and normal visual field at the baseline visit were included. Ocular measurements and fundus photographs were collected every year over the course of the study. Details of the OHTS and the procedure for identifying glaucoma have been outlined in another study.[20] Figure 1 illustrates how fundus photographs were labeled and 3 datasets that we generated from a pool of 66 721 fundus photographs for developing 3 different deep learning models for the detection and prediction of glaucoma. Because of visual field variability, 2 repeated abnormal visual fields were required by the reading center to label the eye as glaucoma. The entire process was reviewed further by an independent end point committee.

The first dataset included 45 379 fundus photographs from nonglaucoma (throughout this article, nonglaucoma refers to eyes with elevated IOP but normal structure and visual field, as defined in the OHTS) eyes and eyes with glaucoma. Of 45 379 fundus photographs, 41 298 were from nonglaucoma eyes and the remaining 4081 photographs were from eyes with glaucoma (determined on the basis of GON or visual field abnormality). We called this the diagnosis dataset (Fig 2, red arrow shows the time points of corresponding fundus photographs). From 4081 fundus photographs from eyes with glaucoma, approximately 29% of these fundus photographs were labeled as glaucoma due to GON without any visual field abnormality, 22% of the photographs were labeled as glaucoma due to visual field abnormality without any evidence of GON, and 49% of photographs were labeled as glaucoma due to existence of both GON and visual field abnormality.

The second dataset included 42 601 fundus photographs from nonglaucoma eyes and eyes that eventually converted to glaucoma after approximately 1 to 3 years. We called this the "late prediction" dataset. The late prediction dataset includes 41 298 fundus photographs from nonglaucoma eyes and 1303 fundus photographs from eyes that converted to glaucoma after 1 to 3 years (Fig 2, yellow arrow shows the time points of corresponding fundus photographs). The third dataset included 42 498 fundus photographs from

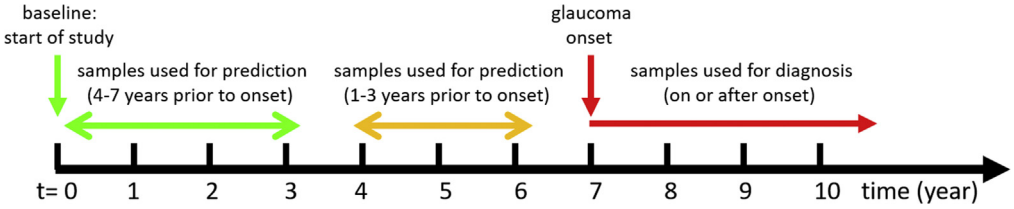

Figure 2. Eyes without any signs of GON or visual field abnormality were followed for approximately 10 years, and fundus photographs were collected annually. The onset time represents when a sample eye was identified as glaucoma based on GON or visual field abnormality. The **green arrow** corresponds to fundus photographs collected 4 to 7 years before the date of glaucoma onset, the **yellow arrow** represents fundus photographs that were collected 1 to 3 years before the date of glaucoma conversion, and the **red arrow** corresponds to fundus photographs collected on or after the time that glaucoma onset was identified.

nonglaucoma eyes and eyes that eventually converted to glaucoma after approximately 4 to 7 years. We called this the "early prediction" dataset. The early prediction dataset included 41 298 fundus photographs from nonglaucoma eyes and 1200 fundus photographs from eyes that eventually developed glaucoma after approximately 4 to 7 years (Fig 2, green arrow shows the time points of corresponding fundus photographs). The same set of fundus photographs obtained from nonglaucoma eyes were used in all 3 datasets. We developed 3 different deep learning models using fundus photographs from these 3 datasets to assess the accuracy of models in predicting and detecting glaucoma.

Train, Test, and Validation Datasets

We first selected 15% of the data for the final validating (retesting). We then selected the rest of 85% of the data and used 5-fold cross-validation for training the models, hyperparameter selection, and testing. In each fold of the cross validation, the 80% of examples from each class were used for training and the remaining examples were used for testing. To avoid bias, all testing and validation were performed on the subject level rather than the eye level without any overlap among train, test, and validation. Repeating this process several times generated reproducible outcomes.

Image Preprocessing

As mentioned earlier, OHTS fundus photographs were scanned from documented fundus photographs (printouts) and saved in JPEG format. Therefore, fundus photographs from the OHTS dataset presented additional artifacts compared with common artifacts present in fundus photographs such as lighting conditions and effects of different environments and camera settings. Artifacts such as image deformation and presence of not-related labels on images are common in images from OHTS dataset. To mitigate some of the image quality issues, we performed contrast enhancement and applied Gaussian filtering to all fundus photographs. The photographs were cropped, normalized, and resized to $224\times224\times3$ (color format).

Deep Learning Model

We used a computationally efficient convolutional neural network (CNN) architecture, the MobileNetV2,[21] to develop our deep learning models. The trainable parameters in MobileNetV2[21] are approximately 1% of the parameters in competing models such as Inception-v3[22] and ResNet-150,[23] making it a great choice for problems where computation resources and the training data are scarce.

The first deep learning model was trained on the "diagnosis dataset," in which fundus photographs had been taken on or after glaucoma onset, and was used to classify a given fundus photograph as glaucomatous or nonglaucomatous (Fig 1). One challenging aspect of this model is to identify fundus photographs that had been labeled as glaucoma due to visual field abnormality without any obvious sign of GON. This makes our diagnosis model more robust compared with previously developed models that only identify fundus photographs that have been labeled as glaucoma due to GON. Likewise, the other 2 models were trained for predicting glaucoma 1 to 3 years and 4 to 7 years before disease onset. To the best of our knowledge, this is among the first attempts at developing deep learning models that can predict glaucoma from fundus photographs several years before clinical functional or structural manifestation of the signs of glaucoma. Because the fundus photographs in the prediction models were collected from eyes before glaucoma onset and therefore without any obvious or clinical signs of glaucoma, prediction models are more challenging to develop than the diagnosis model.

Training Strategy

To train models, we used transfer learning. More specifically, MobileNetV2[21] was initialized with pretrained weights that were initially obtained by training the model on ImageNet dataset. Transfer learning makes the convergence faster and provides a more effective classification performance when dealing with training data with small samples. We then fine-tuned the general knowledge of image interpretation by learning from domain-specific OHTS fundus photographs.

As discussed previously, all 3 datasets had a greater number of fundus photographs from the nonglaucoma eyes compared with glaucoma eyes. On average, 9%, 3.1%, and 2.9% of the fundus photographs in the diagnosis, first, and second prediction datasets were from glaucoma eyes, respectively. To address class imbalance issue, we performed data augmentation and applied balanced data sampling for batch creation. We performed random horizontal and vertical flips, and rotations, and randomly changed the hue, saturation, and contrast of the training fundus photographs. After augmentation, during training, the same number of photographs from both classes were selected for each mini-batch. A batch size of 64 images, cross-entropy loss function, and Adam optimizer (with stochastic regularizer to avoid overfitting) with a fixed learning rate of 0.001 were used for training the models. To further avoid overfitting, weight decay of 0.0001 is used on all layers of the model. All programs were implemented in Python with a backend of PyTorch.

Deep Learning Interpretation

To identify the regions of the fundus photographs that drive the deep learning model to assign an image to glaucoma or

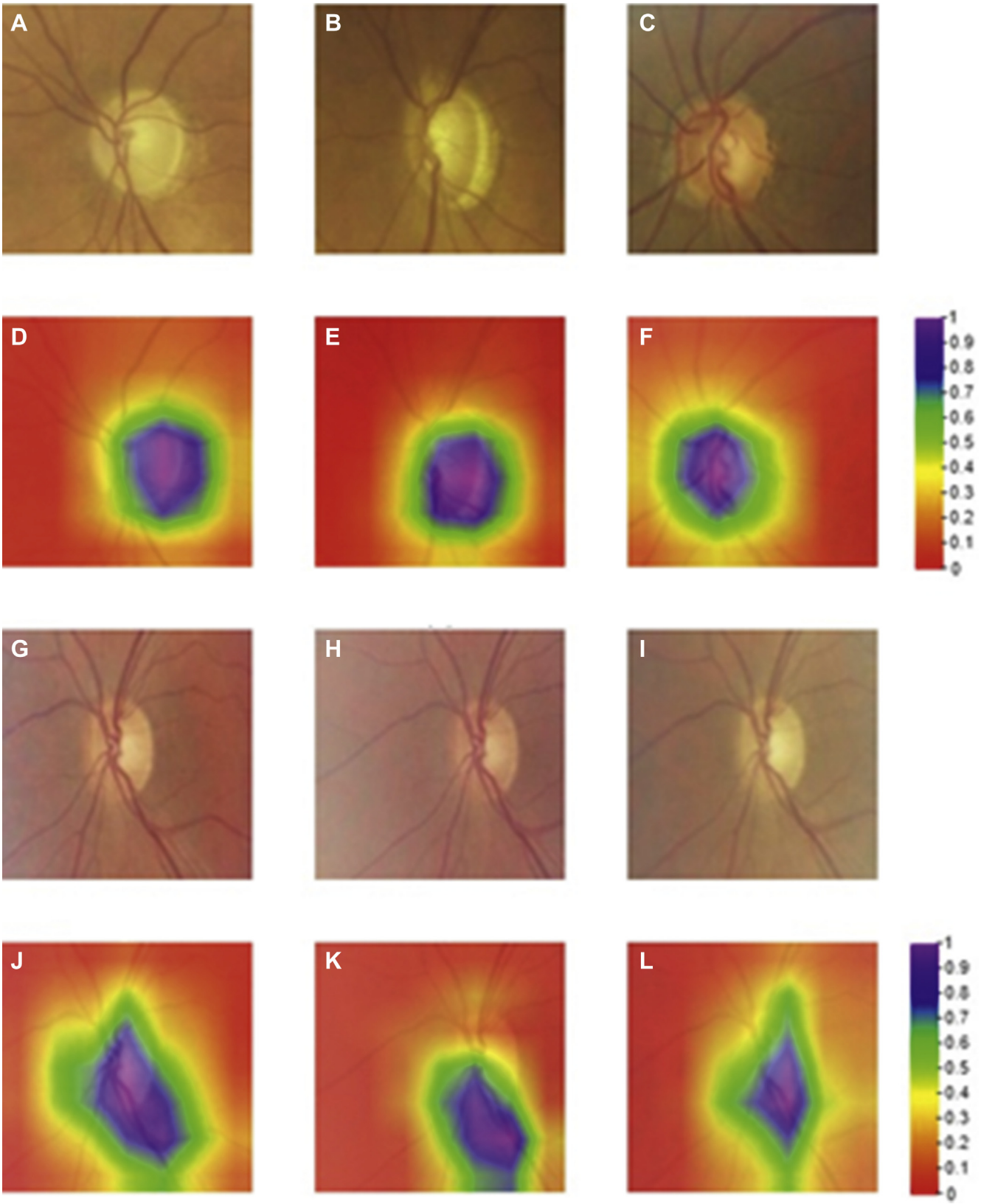

Figure 3. Activation maps representing regions that are most promising for the deep learning model to make a diagnosis. **A-C**: fundus photographs from nonglaucoma eyes. **D-F**: activation maps of fundus photographs of nonglaucoma eyes (shown in the first row). **G-I**: fundus photographs from eyes with glaucoma. **J-L**: activation maps of fundus photographs of eyes with glaucoma (shown in the third row).

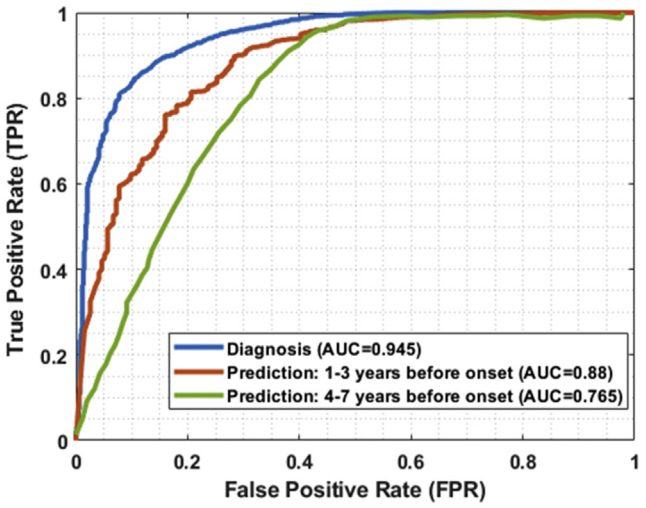

Figure 4. Receiver operating characteristic curves of the prediction and diagnosis models. The **green curve** predicts glaucoma 4 to 7 years before the onset of the disease, the **red curve** predicts glaucoma 1 to 3 years before the onset of the disease, and the **blue curve** shows diagnosing glaucoma on or after onset. AUC = area under the curve.

nonglaucoma groups, we used gradient-weighted class activation maps.[24] The activation maps use the final convolutional layer of a CNN to produce a coarse localization map[24] of the driving regions of the fundus photographs used for diagnosis. Although activation maps can be used to validate deep learning models to verify clinically relevant regions and assess for diagnosis, they also can be used to discover potentially novel biomarkers for the disease.

Statistical Analyses

Models were tested using 5-fold cross-validation datasets (independent from training datasets) and validated (retested) using the held-out dataset. The performance of each model was assessed using area under the curve (AUC). The method of DeLong et al[25] was used to compare the AUC of different models. All statistical analyses were performed in Python.

Results

Approximately 24% of the fundus photographs in the OHTS dataset had extreme artifacts and were excluded from the study. A total of 501 eyes were myopic, defined as spherical equivalent of −1 diopter (D) or more. A total of 195 eyes had myopia equal or worse than −3 D. Figure 3 shows the activation maps obtained from 3 glaucomatous and 3 normal fundus images using the model trained on the diagnosis dataset. As can be seen, activation maps confirm that the optic cup and rim were the most important regions in the input fundus photographs of eyes without glaucoma (Fig 3A-C) and eyes with glaucoma (Fig 3G-I).

Figure 4 shows the receiver operating characteristic curves of the 3 deep learning models that were retested using the held-out subset of the diagnosis, first prediction, and second prediction models, respectively. The AUC of the deep learning model for making diagnosis was 0.945 (95% confidence interval [CI], 0.93−0.96). The AUCs of the deep learning model on the first prediction dataset and second prediction dataset were 0.88 (95% CI, 0.86−0.91) and 0.77 (95% CI, 0.75−0.78), respectively.

For the task of diagnosis, the AUC was improved to 0.97 (95% CI, 0.96−0.98) on retesting fundus photographs that were labeled as glaucoma due to GON. However, as expected, the AUC decreased to 0.88 (95% CI, 0.86−0.89) when we tested the diagnostic deep learning model using the fundus photographs that were labeled as glaucomatous due to abnormal visual field without GON.

Discussion

Unlike in previous studies with the emphasis on diagnosis, we proposed models for prediction of glaucoma before disease onset. The proposed models showed consistent performance in predicting glaucoma development 1 to 3 years and 4 to 7 years before the disease onset. There are several studies that have proposed deep learning for identifying glaucoma from fundus photographs. However, all these methods are centered around glaucoma diagnosis from fundus images that have been collected several years after the initial onset of the disease, whereas in this study, we tackled a more challenging task of predicting glaucoma before manifestation of clinical signs.

Fundus photography provides a simple, inexpensive, and more portable means for screening in underserved populations by nonphysicians, thus improving access to care. Recently, several deep learning approaches have been proposed for detecting glaucoma from fundus photographs. Raghavendra et al[11] developed a deep learning model composed of 18 layers trained and tested on approximately 1500 fundus photographs and were able to reach an accuracy of 98% for diagnosing glaucoma. The AUC of the 6-layer deep learning model for glaucoma diagnosis proposed by Xiangyu et al[12] was 0.83 and 0.88 on 2 different datasets, respectively. Li et al[13] applied a deep learning model using Inception-v3[22] architecture on a large dataset with approximately 40 000 fundus photographs and achieved an AUC of approximately 0.99 in detecting referable glaucoma defined based on GON. Christopher et al[14] developed several deep learning architectures and used a dataset with approximately 14 000 fundus photographs and achieved an AUC of 0.91 in identifying GON eyes. Nourizifard et al (Norouzifard M, et al. Automated glaucoma diagnosis using deep and transfer learning: proposal of a system for clinical testing. Paper presented at: 2018 International Conference on Image and Vision Computing New Zealand (IVCNZ). November 19-21, 2018, Auckland, New Zealand) developed multiple deep learning models and used relatively small datasets with total of approximately 500 fundus photographs and achieved an accuracy of 92%. The reported accuracy of the previous deep learning models to diagnose glaucoma ranges from 0.83 to 0.98.

Except for the studies by Li et al[13] and Christopher et al,[14] the rest of the studies used relatively small datasets of fundus photographs. Therefore, it is challenging to generalize their conclusions. However, we have used 66

721 fundus photographs for training and testing models to develop robust models and generate a reproducible outcome. Aside from large datasets that are required to successfully develop deep learning models, validation is an important step. We have used 3 validation steps: cross-validation, held-out subset, and visualization of promising features through activation maps. Therefore, our models are robust and likely will be generalized to new data.

Although the diagnostic AUC of our model was 0.94, the diagnostic accuracy of the model proposed by Raghavendra et al[11] was 0.98 and the diagnostic AUC of the model proposed by Li et al[13] was 0.99. The lower AUC of our model could be due to several reasons. First, fundus photographs of the OHTS have lower quality compared with the fundus photographs used in other studies. Second, approximately 22% of the fundus photographs in the OHTS were labeled glaucoma due to visual field abnormity without apparent GON. Therefore, it is more challenging to identify glaucomatous eyes without GON from fundus photographs. In fact, our supplemental analysis showed that the AUC will increase to 0.97 if we use only fundus photographs that were labeled as glaucoma due to GON.

Our study used a fully automated model to identify promising glaucoma-induced features (signs), whereas several previous studies used semi-objective hand-engineered features,[26,27] and therefore adopted ad hoc rules. In fact, we showed that by using fully automated CNNs, an AUC of 0.88 can be achieved for predicting glaucoma 1 to 3 years before the manifestations of the clinical signs. Although the human expert may not identify subclinical changes in the optic nerve, the AUC of 0.88 highlights that the optic nerve has gone through subtle changes before the clinical manifestation of the disease. These subtle changes may be identified by a deep learning model but not by a human expert.

The OHTS dataset that was used in our study had several strengths: Participants were recruited from 22 centers across the United States, thereby reducing the idiosyncrasies of local databases; reading centers had access to well-trained certified readers; data were collected, annotated, and cured very well; disease onset was confirmed by repeating image and data collection; and end point committees further confirmed disease onset based on guidelines. Nevertheless, it had several limitations too. One limitation was poor quality of the scanned photographs from documented optic nerve printouts. However, even in the presence of poor quality and high variability, the diagnostic AUC was 0.94, which is promising. The other limitation was the smaller number of eyes with glaucoma eyes compared with non-glaucoma eyes. However, this is a common problem in many healthcare domains and not specific to this study. To address this issue, we used a deep learning model with a relatively small number of parameters, performed data augmentation, and conducted data sampling for balanced batch creation. Another limitation is that the OHTS dataset was collected from a restricted clinical trial and eyes with elevated IOP, and therefore did not represent the general population and real settings. Moreover, only fundus photographs were used to predict glaucoma, whereas several other risk factors may contribute to glaucoma. Therefore, future studies with independent datasets from eye clinics including other glaucoma risk factors may further verify the proposed models.

In conclusion, despite the limitations, our study showed that deep learning models were sufficiently sensitive to predict eyes that will convert to glaucoma from baseline images. This study is an example of how deep learning models may allow us to predict preclinical signs of disease, which may complement other routinely obtained medical examinations. These methods may open new eras in developing deep learning models for predicting glaucoma more accurately and other blinding eye diseases well in advance of the onset of the disease to identify the at-risk population. Our study may also identify previously unknown signatures of the disease development.

References

1. Quigley HA. Number of people with glaucoma worldwide. *Br J Ophthalmol*. 1996;80:389–393.
2. Goldberg I. How common is glaucoma worldwide? In: Weinreb RN, Kitazawa Y, Krieglstein GK, eds. *Glaucoma in the 21st Century*. London: Mosby International; 2000:3–8.
3. Leske MC, Connell AM, Wu SY, et al. Risk factors for open-angle glaucoma. The Barbados Eye Study. *Arch Ophthalmol*. 1995;113:918–924.
4. Coleman AL, Miglior S. Risk factors for glaucoma onset and progression. *Surv Ophthalmol*. 2008;53(Suppl 1):S3–10.
5. Jiang X, Varma R, Wu S, et al. Baseline risk factors that predict the development of open-angle glaucoma in a population: the Los Angeles Latino Eye Study. *Ophthalmology*. 2012;119:2245–2253.
6. Johnson DH. Progress in glaucoma: early detection, new treatments, less blindness. *Ophthalmology*. 2003;110:634–635.
7. Spaeth GL, Reddy SC. Imaging of the optic disk in caring for patients with glaucoma: ophthalmoscopy and photography remain the gold standard. *Surv Ophthalmol*. 2014;59:454–458.
8. Nayak J, Acharya UR, Bhat PS, et al. Automated diagnosis of glaucoma using digital fundus images. *J Med Syst*. 2009;33:337–346.
9. Jampel HD, Friedman D, Quigley H, et al. Agreement among glaucoma specialists in assessing progressive disc changes from photographs in open-angle glaucoma patients. *Am J Ophthalmol*. 2009;147:39–44 e31.
10. Lichter PR. Variability of expert observers in evaluating the optic disc. *Trans Am Ophthalmol Soc*. 1976;74:532–572.
11. Raghavendra U, Fujita H, Bhandary SV, et al. Deep convolution neural network for accurate diagnosis of glaucoma using digital fundus images. *Inform Sci*. 2018;441:41–49.
12. Xiangyu C, Yanwu X, Damon Wing Kee W, et al. Glaucoma detection based on deep convolutional neural network. *Conf Proc IEEE Eng Med Biol Soc*. 2015;2015:715–718.
13. Li Z, He Y, Keel S, et al. Efficacy of a deep learning system for detecting glaucomatous optic neuropathy based on color fundus photographs. *Ophthalmology*. 2018;125:1199–1206.
14. Christopher M, Belghith A, Bowd C, et al. Performance of deep learning architectures and transfer learning for detecting glaucomatous optic neuropathy in fundus photographs. *Sci Rep*. 2018;8:16685.
15. Peng Y, Dharssi S, Chen Q, et al. DeepSeeNet: a deep learning model for automated classification of patient-based age-related

macular degeneration severity from color fundus photographs. *Ophthalmology*. 2019;126:565−575.
16. Burlina PM, Joshi N, Pacheco KD, et al. Use of deep learning for detailed severity characterization and estimation of 5-year risk among patients with age-related macular degeneration. *JAMA Ophthalmol*. 2018;136:1359−1366.
17. Grassmann F, Mengelkamp J, Brandl C, et al. A deep learning algorithm for prediction of age-related eye disease study severity scale for age-related macular degeneration from color fundus photography. *Ophthalmology*. 2018;125:1410−1420.
18. Sayres R, Taly A, Rahimy E, et al. Using a deep learning algorithm and integrated gradients explanation to assist grading for diabetic retinopathy. *Ophthalmology*. 2019;126:552−564.
19. Gulshan V, Peng L, Coram M, et al. Development and validation of a deep learning algorithm for detection of diabetic retinopathy in retinal fundus photographs. *JAMA*. 2016;316:2402−2410.
20. Gordon MO, Kass MA. The Ocular Hypertension Treatment Study: design and baseline description of the participants. *Arch Ophthalmol*. 1999;117:573−583.
21. Sandler M, Howard A, Zhu M, et al. MobileNetV2: Inverted residuals and linear bottlenecks. Paper presented at: 2018 IEEE/CVF Conference on Computer Vision and Pattern Recognition. June 18-23, 2018, Salt Lake City, Utah.
22. Szegedy C, Vanhoucke V, Ioffe S, et al. Rethinking the Inception Architecture for Computer Vision. 2016 IEEE Conference on Computer Vision and Pattern Recognition (CVPR). June 26 to July 1, 2016.
23. He K, Zhang X, Ren S, Sun J. Deep residual learning for image recognition. Paper presented at: 2016 IEEE Conference on Computer Vision and Pattern Recognition (CVPR). June 27-30, 2016.
24. Selvaraju RR, Cogswell M, Das A, et al. Grad-CAM: visual explanations from Deep Networks via gradient-based localization. *2017 IEEE International Conference on Computer Vision (ICCV),* Venice. 2017:618−626. https://doi.org/10.1109/ICCV.2017.74.
25. DeLong ER, DeLong DM, Clarke-Pearson DL. Comparing the areas under two or more correlated receiver operating characteristic curves: a nonparametric approach. *Biometrics*. 1988;44:837−845.
26. Chakrabarty L, Joshi GD, Chakravarty A, et al. Automated detection of glaucoma from topographic features of the optic nerve head in color fundus photographs. *J Glaucoma*. 2016;25:590−597.
27. Annan L, Jun C, Damon Wing Kee W, Jiang L. Integrating holistic and local deep features for glaucoma classification. *Conf Proc IEEE Eng Med Biol Soc*. 2016;2016:1328−1331.

Footnotes and Financial Disclosures

Originally received: January 2, 2020.
Final revision: April 8, 2020.
Accepted: April 21, 2020.
Available online: ■■■. Manuscript no. D-20-00001.

[1] School of Computing and Electrical Engineering, Indian Institute of Technology Mandi, Mandi, Himachal Pradesh, India.

[2] Department of Ophthalmology, University of Tennessee Health Science Center, Memphis, Tennessee.

[3] Department of Ophthalmology, University of California San Diego, San Diego, California.

[4] Department of Genetics, Genomics, and Informatics, University of Tennessee Health Science Center, Memphis, Tennessee.

Financial Disclosure(s):
The author(s) have no proprietary or commercial interest in any materials discussed in this article.

Supported by the National Institutes of Health Grant EY030142 (S.Y.). The funders had no role in study design, data collection and analysis, decision to publish, or preparation of the manuscript.

HUMAN SUBJECTS: Human subjects were included in this study. The fundus photographs in this study were obtained from the ocular hypertension treatment study (OHTS) after signing the data use agreement and receiving the institutional review board (IRB) approval. All research adhered to the tenets of the Declaration of Helsinki. All participants provided informed consent. No animal subjects were used in this study.

Author Contributions

Conception and design: Thakur, Yousefi

Data collection: Thakur, Yousefi

Analysis and interpretation: Thakur, Yousefi

Obtained funding: Yousefi

Overall responsibility: Goldbaum, Yousefi

Abbreviations and Acronyms:
AUC = area under the curve; **CI** = confidence interval; **CNN** = convolutional neural network; **D** = diopter; **GON** = glaucomatous optic neuropathy; **IOP** = intraocular pressure; **OHTS** = Ocular Hypertension Treatment Study.

Correspondence:
Siamak Yousefi, PhD, 930 Madison Ave., Suite 726, Memphis, TN 38163. E-mail: siamak.yousefi@uthsc.edu.